Stable vortex solitons supported by competing quadratic and cubic nonlinearities

D. Mihalache,[1,2] D. Mazilu,[1,2] B. A. Malomed,[3] and F. Lederer[2]
[1]*Department of Theoretical Physics, Institute of Atomic Physics, P.O. Box MG-6, Bucharest, Romania*
[2]*Institute of Solid State Theory and Theoretical Optics, Friedrich-Schiller Universität Jena, Max-Wien-Platz 1, D-07743, Jena, Germany*
[3]*Department of Interdisciplinary Studies, Faculty of Engineering, Tel Aviv University, Tel Aviv 69978, Israel*
(Received 1 December 2003; revised manuscript received 17 March 2004; published 17 June 2004)

We address the stability problem for vortex solitons in two-dimensional media combining quadratic and self-defocusing cubic $[\chi^{(2)}:\chi_{-}^{(3)}]$ nonlinearities. We consider the propagation of spatial beams with intrinsic vorticity S in such bulk optical media. It was earlier found that the $S=1$ and $S=2$ solitons can be stable, provided that their power (i.e., transverse size) is large enough, and it was conjectured that all the higher-order vortices with $S\geqslant 3$ are always unstable. On the other hand, it was recently shown that vortex solitons with $S>2$ and very large transverse size may be stable in media combining cubic self-focusing and quintic self-defocusing nonlinearities. Here, we demonstrate that the same is true in the $\chi^{(2)}:\chi_{-}^{(3)}$ model, the vortices with $S=3$ and $S=4$ being stable in regions occupying, respectively, $\simeq 3\%$ and 1.5% of their existence domain. The vortex solitons with $S>4$ are also stable in tiny regions. The results are obtained through computation of stability eigenvalues, and are then checked in direct simulations, with a conclusion that the stable vortices are truly robust ones, easily self-trapping from initial beams with embedded vorticity. The dependence of the stability region on the $\chi^{(2)}$ phase-mismatch parameter is specially investigated. We thus conclude that the stability of higher-order two-dimensional vortex solitons in narrow regions is a generic feature of optical media featuring the competition between self-focusing and self-defocusing nonlinearities. A qualitative analytical explanation to this feature is proposed.

DOI: 10.1103/PhysRevE.69.066614 PACS number(s): 42.65.Tg

I. INTRODUCTION

Optical vortex beams have attracted much attention in the last decade because of possible applications to all-optical processing of information (where they may play the role of reconfigurable conduits guiding weak signal beams [1,2]) and, in a more general context, as delocalized (dark) or localized (bright) topological optical solitons in various two-dimensional (2D) [3–18] and three-dimensional (3D) [19–21] settings (for a recent review of theoretical and experimental results in this field, see the book [22]). Other promising applications of optical vortices are trapping and channeling of matter waves, as well as capture and controlled transport of microparticles, which are trapped by the dark ("empty") core of the vortex beam [23], or absorption of particles in spinning motion (by transfer of the angular momentum from the beam) [24]. Very recently, formation of stable bright vortex solitons (spatially localized vortex beams) was observed experimentally, for the first time, in anisotropic photorefractive media through self-trapping of partially incoherent light carrying a phase dislocation [25] (experiments with *unstable* vorticity-carrying localized beams were reported in both $\chi^{(2)}$ crystals [26] and in media with a saturable nonlinearity (a hot, dense sodium vapor) [27]).

In fact, stability is a major concern for bright vortex solitons, as, unlike their zero-spin counterparts, they are prone to instability against azimuthal perturbations breaking the axial symmetry. A general problem in the study of the azimuthal instability is that it is an oscillatory one, i.e., the associated eigenvalues are complex, and the instability cannot be predicted by dint of known general principles, such as the Vakhitov-Kolokolov (VK) criterion [28], which applies to the case of real instability eigenvalues. In 2D and 3D models with quadratic $[\chi^{(2)}]$ nonlinearities, this instability was discovered in simulations [20,29], and observed in the above-mentioned experiment in the 2D case [26]. As a result, a vortex ("spinning") soliton with vorticity ("spin") $S=1$ splits into three or two fragments in the form of separating zero-spin solitons, so that the initial intrinsic spin momentum is transformed into the orbital momentum. Nevertheless, the $\chi^{(2)}$ nonlinearity acting in combination with the self-*defocusing* Kerr (alias $\chi_{-}^{(3)}$, where we use the subscript "minus" to stress the self-defocusing) nonlinearity gave rise to the first examples of *stable* spinning (ring-shaped) 2D solitons with $S=1$ and $S=2$ [16]. Actually, $\chi^{(2)}:\chi_{-}^{(3)}$ nonlinear-optical models in the spatial domain had been known before the investigation of the vortex solitons started [30,31] (possibilities for experimental implementation of the $\chi^{(2)}:\chi_{-}^{(3)}$ optical nonlinearities, chiefly based on the quasi-phase-matching technique, were discussed in Refs. [16,32]).

The stability of the spinning solitons in this model may be realized as a result of competition between the self-focusing and self-defocusing nonlinearities. This understanding is further supported by the fact that similar stable spinning solitons have also been found in another optical model featuring the competition between focusing and defocusing nonlinearities, viz., the one based on the cubic-quintic (CQ) nonlinear Schrödinger equation [6–12]. In fact, stable spinning solitons were first identified in this model [6].

A principally important issue is to identify values of the spin S at which the 2D vortex solitons may be stable. In the CQ model, only stable solitons with $S=1$ were originally identified [6]. Then, it was found that $S=2$ vortices have

their stability region, too [7,8]. Finally, it was demonstrated that the vortex solitons in the CQ model may be stable with the values of spin up to $S=5$ [11]; quite plausibly, very narrow stability regions exist for any value of S in the CQ model. On the other hand, in the $\chi^{(2)}:\chi_{-}^{(3)}$ model stable spinning solitons were thus far found only for $S=1$ and $S=2$ [16], which suggests to seek for stable solitons with $S>2$ in this model, too. The most important aspect of the problem is to understand whether the existence of stable spinning solitons with higher values of S is a peculiarity of the CQ model or a generic feature. Another challenge, which is also an aim of the present work, is to develop a qualitative explanation for the stability of vortex solitons. Finally, a noteworthy corollary to the stability results for $S>1$ is that, in the models with competing nonlinearities, dark solitons with multiple values of the topological charge, which may be considered as a limiting case of the bright ones with an infinitely large size, are *stable*, too (while in the well-known model with the self-defocusing $\chi_{-}^{(3)}$ nonlinearity, all dark vortices with $S>1$ are unstable [33]).

The paper is organized as follows. In Sec. II, the model is formulated, and general results concerning the existence of 2D bright vortex solitons in it with different values of S are presented. The fundamental results for the stability of the spinning solitons, based on calculation of eigenvalues found from equations linearized around the soliton solutions, are reported in Sec. III. Direct simulations of the solitons' stability within the framework of the full nonlinear evolution equations, which confirm the results based on the eigenvalues, are displayed in Sec. IV. In Sec. V, we propose a qualitative explanation of the stability of the vortex solitons, including the fact that the stability region drastically shrinks with the increase of S. Section V concludes the work.

II. THE MODEL AND SPINNING SOLITONS

Equations describing the $\chi^{(2)}$ coupling between the fundamental-frequency (FF) and second-harmonic (SH) fields u and v in the presence of the self-defocusing $\chi^{(3)}$ nonlinearity in the $(2+1)$-dimensional geometry are well known [16,30,31,34–36]:

$$i\frac{\partial u}{\partial Z}+\frac{1}{2}\nabla^2 u+u^{*}v-(|u|^2+2|v|^2)u=0,$$
$$i\frac{\partial v}{\partial Z}+\frac{1}{2}\nabla^2 v+\beta v^{*}u^2-2(2|u|^2+|v|^2)u=0. \tag{1}$$

Here * stands for the complex conjugation, Z is the propagation distance, ∇^2 is the diffraction operator acting on the normalized transverse spatial coordinates X and Y, and β is a phase-mismatch parameter. Equations (1) assume that the Poynting-vector walk-off between the harmonics is compensated [36,37].

We look for stationary solutions to Eqs. (1) in the form of

$$u=U(r)\exp(i\kappa Z+iS\theta),\quad v=V(r)\exp[2(i\kappa Z+iS\theta)],$$

where (r,θ) are the polar coordinates in the plane (X,Y), κ is the wave number, and the integer S is the above-mentioned spin. The amplitudes U and V may be assumed real, obeying the equations

$$(U''+r^{-1}U'-S^2r^{-2}U)-2[\kappa U-UV+(U^2+2V^2)U]=0,$$
$$(V''+r^{-1}V'-4S^2r^{-2}V)-4[(2\kappa+\beta)V-U^2+2(2U^2+V^2)V]=0, \tag{2}$$

where the prime stands for d/dr.

The dynamical equations (1) conserve the total power (norm),

$$E=\int(|u|^2+|v|^2)dXdY\equiv E_u+E_v, \tag{3}$$

Hamiltonian

$$H=\frac{1}{2}\int\int\left[|\nabla u|^2+\frac{1}{4}|\nabla v|^2+\beta|v|^2-(u^{*2}v+u^2v^{*})+|u|^4+4|u|^2|v|^2+|v|^4\right]dXdY, \tag{4}$$

momentum (equal to zero for the solutions considered), and angular momentum in the transverse plane [38,39],

$$L=\int\int\left(\frac{\partial\phi}{\partial\theta}|u|^2+\frac{\partial\psi}{\partial\theta}|v|^2\right)dXdY,$$

where ϕ and ψ are phases of the complex fields u and v. The following relations between L, H, and E for a stationary spinning soliton follow from Eqs. (2): $L=SE$, and

$$H=-\frac{1}{2}\kappa E+\frac{1}{4}\beta E_v-\frac{1}{4}\int\int(|u|^4+4|u|^2|v|^2+|v|^4)dXdY. \tag{5}$$

We have numerically found one-parameter families of stationary 2D spinning solitons having a ring-like shape with a hole in its center, which is supported by the phase dislocation. To this aim, we solved Eqs. (2) using the standard band-matrix algorithm [40] to deal with the corresponding two-point boundary-value problem.

Obviously, the wave number κ must exceed the cutoff value, $\kappa\geqslant\kappa_{\mathrm{cutoff}}\equiv\max\{0,-\beta/2\}$, for the fields to be exponentially localized. For a fixed mismatch β, the stationary zero-spin and spinning solitons exist in a limited region, with κ ranging from κ_{cutoff} up to a certain upper limit (offset value) κ_{offset}, at which the soliton's power diverges due to the divergence of its outer radius R, while the field amplitudes U and V remain finite. As it follows from Eqs. (2), the limiting values of the amplitudes U_0 and V_0 corresponding to $\kappa=\kappa_{\mathrm{offset}}$ are related to as follows:

$$\kappa_{\mathrm{offset}}=\frac{V_0}{2V_0-1}(\beta-1+6V_0-6V_0^2), \tag{6}$$

$$U_0^2=-\kappa_{\mathrm{offset}}+V_0-2V_0^2 \tag{7}$$

[it follows from Eq. (7) that κ_{offset} must take values smaller than $1/8$, otherwise U_0^2 cannot be positive]. Further straight-

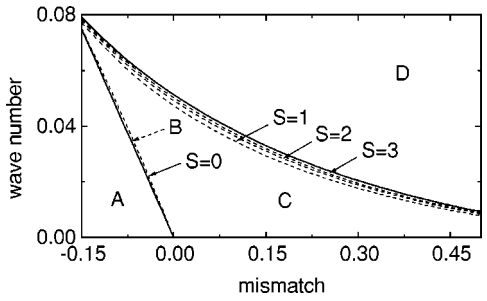

FIG. 1. Existence and stability domains for bright fundamental and vortex solitons with $S=0$, 1, 2, and 3. The upper continuous curve separating the domains C and D is their common existence border, corresponding to infinitely broad solitons. The stability region of the vortices with $S=4$, which is very narrow, is explained in the text.

forward analysis of Eqs. (2) shows that R diverges logarithmically at $\kappa_{\text{offset}}-\kappa\to 0$,

$$R \sim \ln[1/(\kappa_{\text{offset}}-\kappa)]. \tag{8}$$

These results are summarized in Fig. 1, where the continuous lines border the existence domain of the localized ring-shaped solitons, and the dashed lines are boundaries between stable and unstable regions in the parameter plane (β,κ). The way the stability boundaries were identified will be explained in the following section. In regions A and D in Fig. 1, no localized solutions exists: in region A—because the wave number κ is below the cutoff, and in region D—because the defocusing $\chi^{(3)}$ nonlinearity becomes dominant, preventing the formation of solitons. For $\beta<0$, there is a narrow strip (region B in Fig. 1) where the zero-spin solitons exist but are unstable. Stable zero-spinning and unstable spinning solitons coexist in region C. Stable spinning solitons with $S=1$, $S=2$, *and* $S\geqslant 3$ exist in small domains near the offset line (the continuous line separating regions C and D), the dashed lines located near the offset line being boundaries of the stability regions for the spinning solitons. We have found that, regardless of the value of the phase mismatch, the spinning solitons with $S=3$ and $S=4$ are stable in regions occupying $\simeq 3\%$, respectively $\simeq 1.5\%$ of their existence domain.

In Figs. 2 and 3 we plot dependences $\kappa=\kappa(E)$ and $H=H(E)$ for *both* nonspinning and spinning solitons for two representative values of the mismatch β. The full and dashed lines in Figs. 2 and 3 correspond to stable and unstable branches according to results presented below. In particular, the zero-spin solitons are stable according to the above-mentioned Vakhitov-Kolokolov (VK) criterion, which states that a *necessary* stability condition for solitons of any type is $dE/d\kappa>0$ [28]. Actually, the VK criterion may play the role

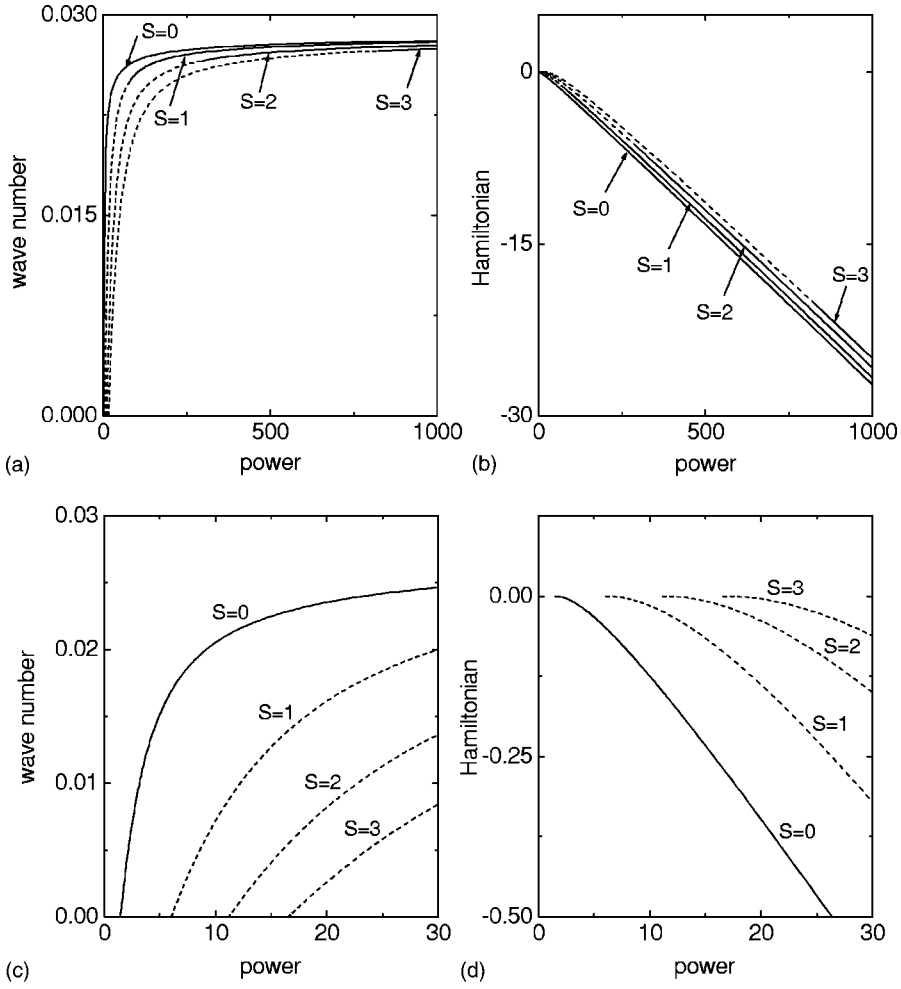

FIG. 2. The wave number κ (a) and Hamiltonian H (b) of the vortex solitons, with different values of spin, versus their power E, with the phase mismatch $\beta=0.2$. Panels (c) and (d) are blowups of small-power regions from panels (a) and (b).

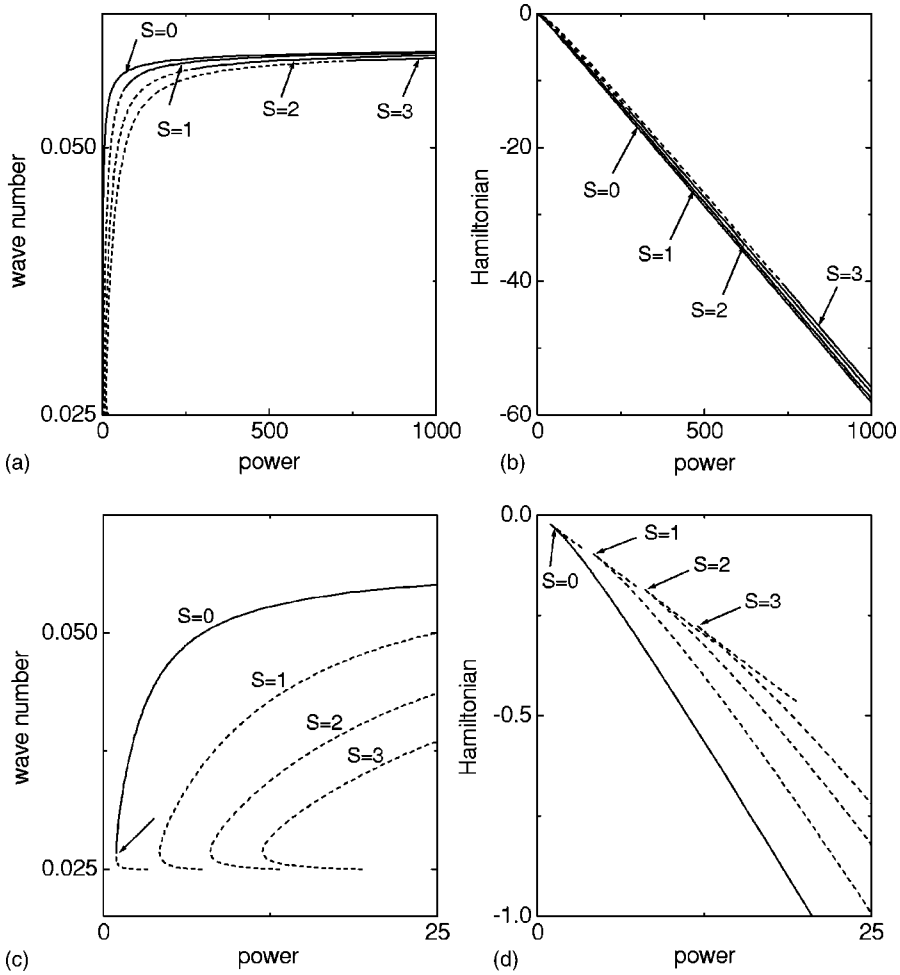

FIG. 3. The same as in Fig. 2, but for phase mismatch $\beta=-0.05$.

of a sufficient one for zero-spin solitons; however, it ignores a possibility of azimuthal instabilities, which are often fatal for bright vortex solitons.

An essential feature, which is evident in Figs. 2 and 3, is that both the zero-spin and spinning solitons cannot exist unless the power E exceeds the corresponding threshold value $E_{\rm thr}^{(S)}$, at both positive and negative values of the phase mismatch. For example, in the case of $\beta=0.02$, $E_{\rm thr}^{(0)}=1.48$, $E_{\rm thr}^{(1)}=6.05$, $E_{\rm thr}^{(2)}=11.30$, and $E_{\rm thr}^{(3)}=16.70$ (see Fig. 2). For $\beta>0$, the soliton's wave number increases monotonically with the power towards the maximum value $\kappa_{\rm offset}$. For $\beta<0$, we observe two branches in the wave number–power diagram, one with the power decreasing monotonically with κ in narrow regions above the cutoff, hence all the corresponding solitons (zero-spin and spinning ones) are unstable according to the VK criterion (dashed lines in Fig. 3), and another branch with the power increasing monotonically with κ (see Fig. 3). For the typical examples shown in Figs. 2 and 3, the offset values are $\kappa_{\rm offset}=0.0283$ for $\beta=0.2$, and $\kappa_{\rm offset}=0.0592$ for $\beta=-0.05$.

Typical shapes of *stable* bright vortex solitons are displayed in Figs. 4 and 5. These figures include cases close to the instability border [Figs. 4(a) and 5(a)], and ones near the offset limits [Figs. 4(b) and 5(b)]. The stable bright vortex soliton resembles a dark vortex, bounded at a large value of the radius by a circular kink-like layer, so that stable vortex solitons exhibit a flat-top shape with the hole in the center. Notice that stable vortex solitons with a flat-top shape are also known in models of dissipative media described by the two-dimensional Ginzburg-Landau equations with the CQ nonlinearity [14].

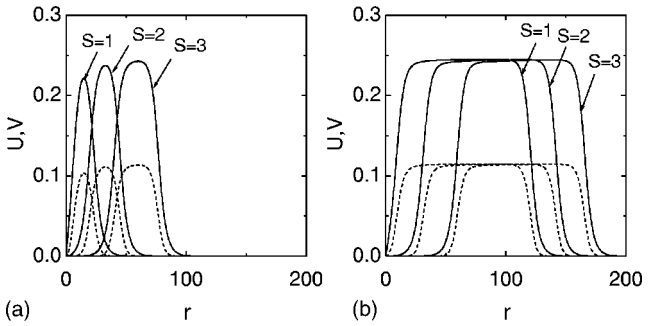

FIG. 4. Typical shapes (shown by means of their radial cross sections) of stable vortex solitons for $\beta=0.2$: (a) $\kappa=0.025$ for $S=1$, $\kappa=0.0265$ for $S=2$, and $\kappa=0.0273$ for $S=3$; (b) $\kappa=0.0279$ for $S=1$, $S=2$, and $S=3$. Full lines: the fundamental-frequency field U; dashed lines: the second-harmonic field V.

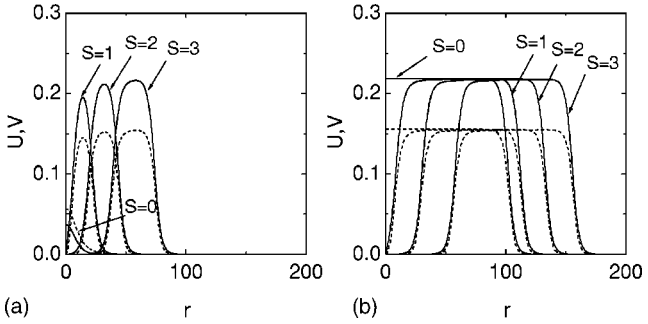

FIG. 5. The same as in Fig. 4 but for $\beta=-0.05$: (a) $\kappa=0.027$ for $S=0$, $\kappa=0.0556$ for $S=1$, $\kappa=0.0573$ for $S=2$, and $\kappa=0.0581$ for $S=3$; (b) $\kappa=0.0592$ for $S=0$, $S=1$, $S=2$, and $S=3$.

III. LINEAR STABILITY ANALYSIS OF SPINNING SOLITONS

The revealing information on the stability of solitons is provided by calculation of eigenvalues within the framework of the underlying equations (1) linearized about the stationary spinning-soliton solutions. To this end, we seek for infinitesimal perturbation eigenmodes in the general form,

$$u(Z,r,\theta) - U(r)\exp[i(S\theta+\kappa Z)] \tag{9}$$

$$= f(r)\exp\{\lambda_n Z + i[(S+n)\theta+\kappa Z]\} + g^*(r)\exp\{\lambda_n^* Z + i[(S-n)\theta+\kappa Z]\}, \tag{10}$$

$$v(Z,r,\theta) - V(r)\exp[2i(S\theta+\kappa Z)] \tag{11}$$

$$= p(r)\exp\{\lambda_n Z + i[(2S+n)\theta+2\kappa Z]\} + q^*(r)\exp\{\lambda_n^* Z + i[(2S-n)\theta+2\kappa Z]\}, \tag{12}$$

where $n>0$ is an arbitrary integer azimuthal index of the perturbation, λ_n is the (complex) eigenvalue sought for, and the functions f, g and p, q obey linear equations

$$i\lambda_n f + \tfrac{1}{2}[f'' + r^{-1}f' - (S+n)^2 r^{-2} f] - \kappa f - 2(U^2+V^2)f - (U^2-V)g - (2UV-U)p - 2UVq = 0,$$

$$-i\lambda_n g + \tfrac{1}{2}[g'' + r^{-1}g' - (S-n)^2 r^{-2} g] - \kappa g - 2(U^2+V^2)g - (U^2-V)f - (2UV-U)q - 2UVp = 0,$$

$$i\lambda_n p + \tfrac{1}{4}[p'' + r^{-1}p' - (2S+n)^2 r^{-2} p] - (2\kappa+\beta)p - 4(U^2+V^2)p - 2V^2 q - 2(2UV-U)f - 4UVg = 0,$$

$$-i\lambda_n q + \tfrac{1}{4}[q'' + r^{-1}q' - (2S-n)^2 r^{-2} q] - (2\kappa+\beta)q - 4(U^2+V^2)q - 2V^2 p - 2(2UV-U)g - 4UVf = 0.$$

The solutions for f, g, p, and q must decay exponentially at $r\to\infty$, and at $r\to 0$ their asymptotic form must be, respectively, $\sim r^{|S+n|}$, $r^{|S-n|}$, $r^{|2S+n|}$, and $r^{|2S-n|}$. To solve the linear equations and find the eigenvalues, we used a known numerical procedure [29,41], which produces results presented in Figs. 6–8.

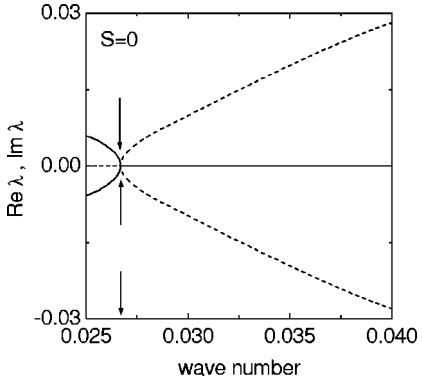

FIG. 6. The bifurcation diagram accounting for the stability change of the fundamental ($S=0$) soliton at negative phase mismatch ($\beta=-0.05$). Full and dashed lines show the real and imaginary parts of the eigenvalues. The arrows indicate the stability-change point, $\kappa_{st}\approx 0.026\,69$. This figure and the two following ones show the full region, $\kappa_{cutoff}<\kappa<\kappa_{offset}$, in which the corresponding vortex solitons exist.

The output of numerical calculations for a typical zero-spin soliton is presented in Fig. 6. The relevant eigenvalues are either real or pure imaginary (in fact, in this case they can be found by means of asymptotic expansions around zero modes induced by the translational, rotational, and phase-shift symmetries). The arrows in Fig. 6 point to the stability-change bifurcation at $\kappa=\kappa_{st}=0.026\,69$ (for $\beta=-0.05$), which (up to the accuracy of the numerical data) exactly coincides with the critical point predicted by the VK criterion in this case. The bifurcation scenario accounting for the destabilization of the zero-spin solitons is the standard one: two imaginary eigenvalues collide at the origin, giving rise to a pair of real eigenvalues with opposite signs.

In Fig. 7 we plot the output of comprehensive numerical calculations of complex eigenvalues responsible for the bifurcation (of the *Hamiltonian-Hopf* type) which accounts for the stability change of spinning solitons with $S=3$, for a typical value of the positive mismatch, $\beta=0.2$. The corresponding eigenvalues appear in quartets, $(\lambda,\lambda^*,-\lambda,-\lambda^*)$, as the system is conservative, cf. earlier known results for scalar [11,42] and vectorial vortex solitons [43,44]. For a given azimuthal mode, the unstable complex quartet is generated by a collision between pairs of stable imaginary eigenvalues, which is typical to the Hamiltonian-Hopf bifurcation.

We stress that the case of $S=3$, the results for which are displayed above, is a new one, as compared to those with $S=1$ and $S=2$, which were studied earlier in this model [16]. We also studied in detail higher values of S, arriving at results quite similar to those presented in Fig. 7. In particular, for $S=4$ we have found that the stability changes at the critical point $\kappa_{st}=0.058\,71$ for $\beta=-0.05$, and at $\kappa_{st}=0.027\,86$ for $\beta=0.02$, resulting in a narrow stability domain.

The mechanism for the stability change, as the wave number κ passes the critical value κ_{cr}, is again the collision between pairs of imaginary eigenvalues as outlined above, and it is always accounted for by the perturbation eigenmodes pertaining to the azimuthal index $n=2$ (cf. a discussion in Ref. [11] of the stability-instability transition for spinning solitons with $S\geqslant 3$ in the CQ model).

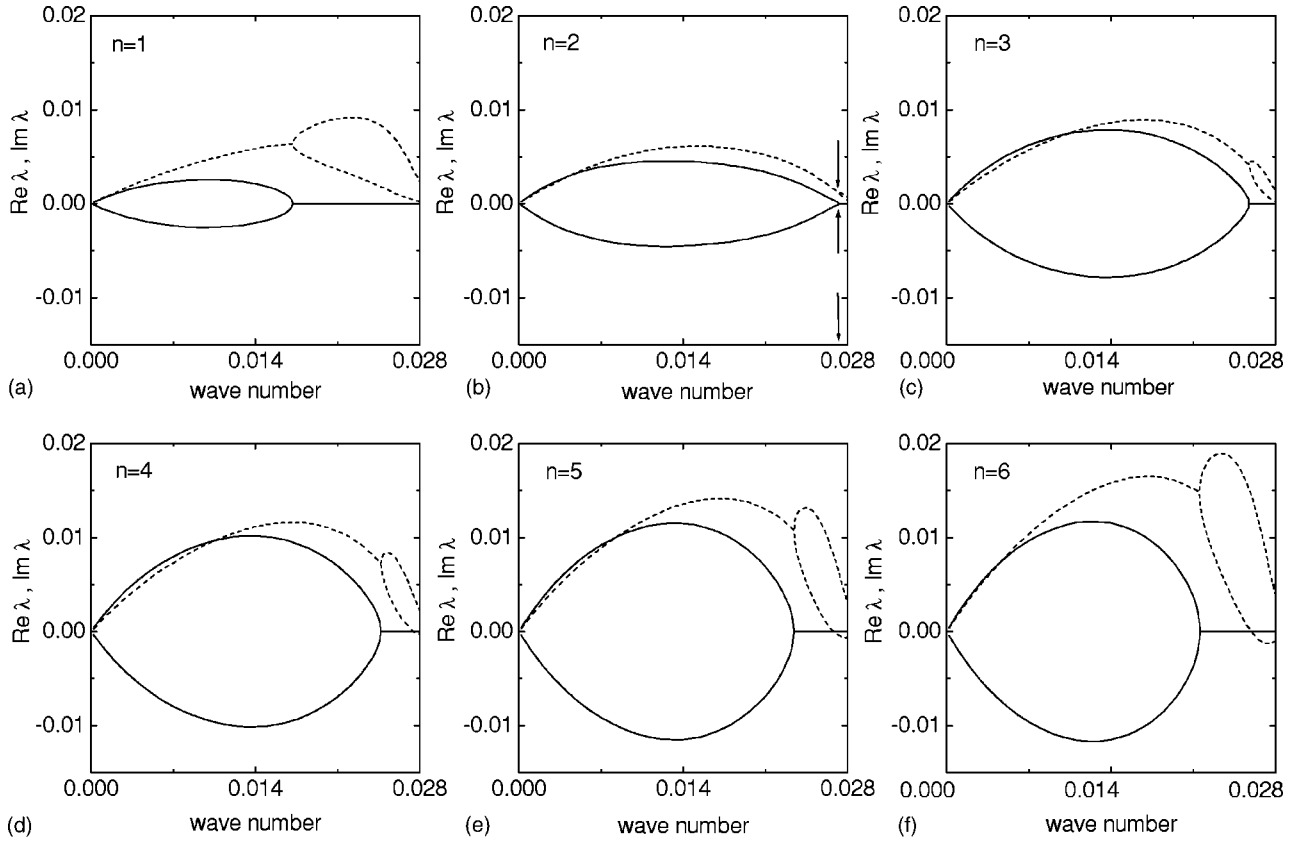

FIG. 7. Bifurcation diagrams accounting for the stability of the newly found vortex solitons with $S=3$ and $\beta=0.2$ (recall that previous works reported only stable solitons with $S=1$ and $S=2$ in the present model). The panels show the real and imaginary (full and dashed lines) parts of the eigenvalues, which correspond to perturbation eigenmodes with the azimuthal indices $n=1,2,3,4,5$, and 6, versus the wave number κ. As is seen, the most dangerous eigenmode is the one with $n=2$ (panel b). The arrows in this panel mark the position of the stability-change point for the solitons with $S=3$.

These results suggest that the vortex solitons with *any* value of S may be stable, provided they are sufficiently broad, as $\kappa \to \kappa_{\text{offset}}$ implies the divergence of the soliton's outer radius R, as per Eq. (8). When the instability disappears with the increase of κ, i.e., the real part of the corresponding eigenvalue vanishes, its imaginary part remains finite, as explained above (see Fig. 7). This fact explains why the azimuthal instability, crucial for the vortex solitons, cannot be captured by asymptotic expansions around zero modes generated by the above-mentioned symmetries of the system (such asymptotic expansions are, as a matter of fact, the basis of the VK criterion, which detects only instabilities accounted for by purely real eigenvalue pairs).

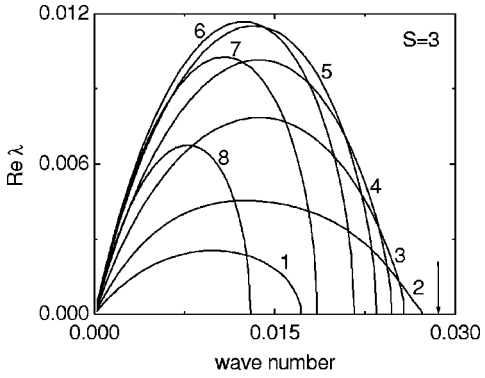

FIG. 8. The instability growth rate, Re λ, corresponding to different values of the perturbation azimuthal index n (indicated by labels near the curves) versus the soliton's wave number κ for $\beta=0.2$ and $S=3$. The largest instability growth rate corresponds to $n=6$, while the most persistent instability pertains to $n=2$. The latter vanishes at $\kappa=\kappa_{\text{st}}=0.0273$. The border of the existence region for the bright solitons, $\kappa=\kappa_{\text{offset}}$, is marked by the vertical arrow.

Figure 7 demonstrates that, for the solitons with $S=3$, the stability region occupies 3.6% of their existence domain [the arrows in Fig. 7(b) mark the edge of the stability region for the $S=3$ solitons; we define its relative width as $\epsilon \equiv (\kappa_{\text{offset}} - \kappa_{\text{st}})/(\kappa_{\text{offset}} - \kappa_{\text{cutoff}})$]. For comparison, previously known results imply that $\epsilon \simeq 11.8\%$ for $S=1$, and $\epsilon \simeq 6.4\%$ for $S=2$ (see Fig. 2). In the case of the negative mismatch ($\beta<0$), the stability region is slightly smaller: if $\beta=-0.05$, it is $\epsilon \simeq 10.6\%$ for $S=1$, $\epsilon \simeq 5.7\%$ for $S=2$, and $\epsilon \simeq 2.9\%$ for $S=3$. For $S=4$, the relative stability interval size is $\simeq 1.6\%$ for $\beta=0.2$, and $\simeq 1.3\%$ for $\beta=-0.05$. We thus infer that the relative width of the stability region strongly shrinks with the increase of S. Below, a qualitative explanation will be given to this feature.

Figure 8 shows a summary of the calculation of the real part of the relevant eigenvalues for the $S=3$ solitons, pertaining to the azimuthal indices up to $n=8$. Similar results for the solitons with $S=1$ and $S=2$ were reported in Ref. [16].

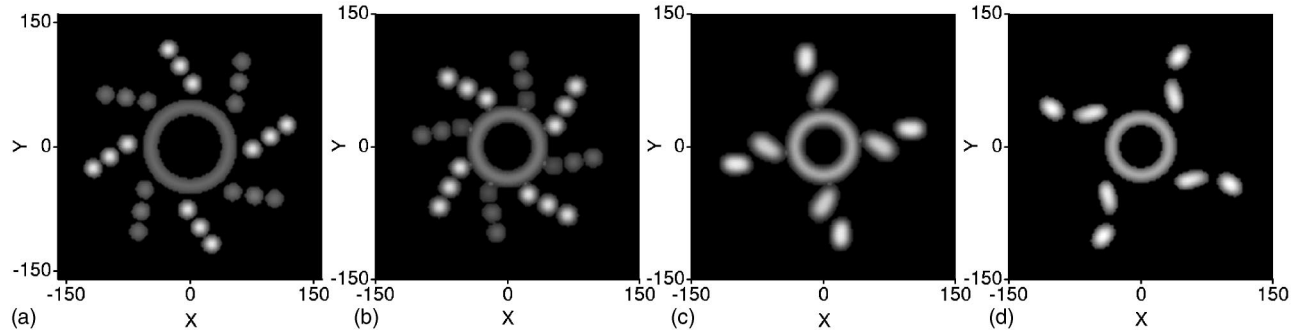

FIG. 9. Fragmentation of an unstable $S=3$ soliton into a set of zero-spin ones, as a result of the azimuthal instability. In this case, $\beta=0.2$ and (a) $\kappa=0.005$, (b) $\kappa=0.010$, (c) $\kappa=0.016$, and (d) $\kappa=0.020$. Here and in Figs. 11 and 12, only the FF component of the wave field is shown; the SH component displays a similar behavior.

Lastly, the transition to the stability for all values of S for $\kappa \to \kappa_{\text{offset}}$ clearly implies that dark vortices, which may be regarded as the limiting case of the bright ones with the infinite radius, are stable for any S. This is a drastic difference from the well-known dark vortices in the model with the self-defocusing Kerr $[\chi_{-}^{(3)}]$ nonlinearity, where only the fundamental vortices with $S=1$ are stable [33].

IV. DIRECT SIMULATIONS

The stability predictions based on the eigenvalues found from the linearized equations were checked against direct simulations of the full equations (1). The simulations were carried out by means of the Crank-Nicholson scheme. The system of nonlinear finite-difference equations was first solved by means of the Picard iteration method [45], and the resulting linear system was then handled with the Gauss–Seidel iterative scheme. For good convergence we needed, typically, five Picard iterations and six Gauss-Seidel iterations. We employed a transverse grid with 1001×1001 points, and the typical longitudinal step size was $\Delta Z=0.08$. To avoid distortion of the instability development under the action of the periodicity imposed by the Cartesian computational mesh, we added initial perturbations that were mimicking random fluctuations in a real system (cf. Ref. [46]).

The development of the instability of the spinning solitons with $S=3$ (in the case when it is unstable) is illustrated by Fig. 9 for four values of the wave number κ. Here we superimpose a succession of images of the transverse intensity distribution at different values of the propagation distance Z. As is seen, the azimuthal instability breaks up the unstable spinning soliton into a set of zero-spin ones, which fly out tangentially relative to the circular crest of the original ring-shaped soliton. Thus, the initial intrinsic angular momentum (spin) of the vortex soliton is converted into the orbital momentum of the emerging nonspinning fragments. We have found that the number of the emerging fragments depends on the wave number κ: it ranges between eight, in Figs. 9(a) and 9(b), and four in Figs. 9(c) and 9(d). Moreover, for given κ, the number of the emerging fragments is *not* necessarily equal to the azimuthal index of the perturbation having the largest growth rate at the same value of κ (see Fig. 8).

In order to test the robustness of the stable vortex soliton with $S=3$ in a more general context, corresponding to the situation in the physical experiment, random noise was added at input. For two representative values of the phase mismatch β, in Fig. 10 we show the evolution of the soliton's power E and Hamiltonian H during the process of noise self-cleaning by the stable soliton with $S=3$ which was perturbed at input (the decrease of E and H implies not violation of the conservation laws, but separation between the soliton and noise ejected by it, as the power and Hamiltonian, shown in this figure, are computed only for the area occupied by the soliton). Figure 11 shows that the stable vortex soliton was able to completely heal the damage incurred by the initial perturbation, proving itself a truly stable object.

To further illustrate the physical purport of the stable vortex solitons with $S=3$, in Fig. 12 we display its self-trapping from an input Gaussian beam with a nested vortex, whose

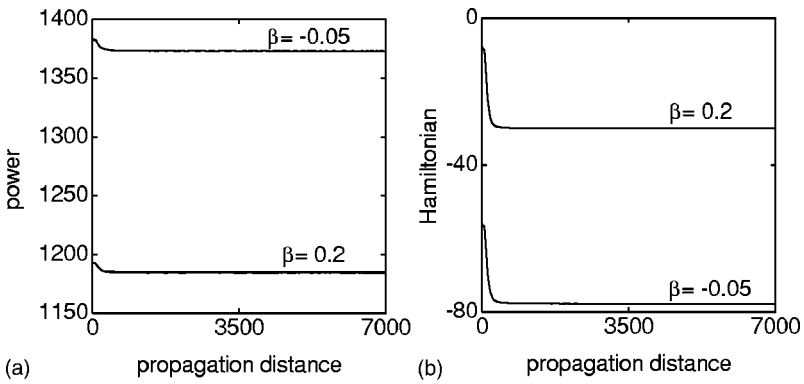

FIG. 10. Evolution of the total power E (a) and Hamiltonian H (b) of the stable soliton with spin $S=3$, perturbed at input. Here, $\kappa=0.0586$ for $\beta=-0.05$, and $\kappa=0.0276$ for $\beta=0.2$.

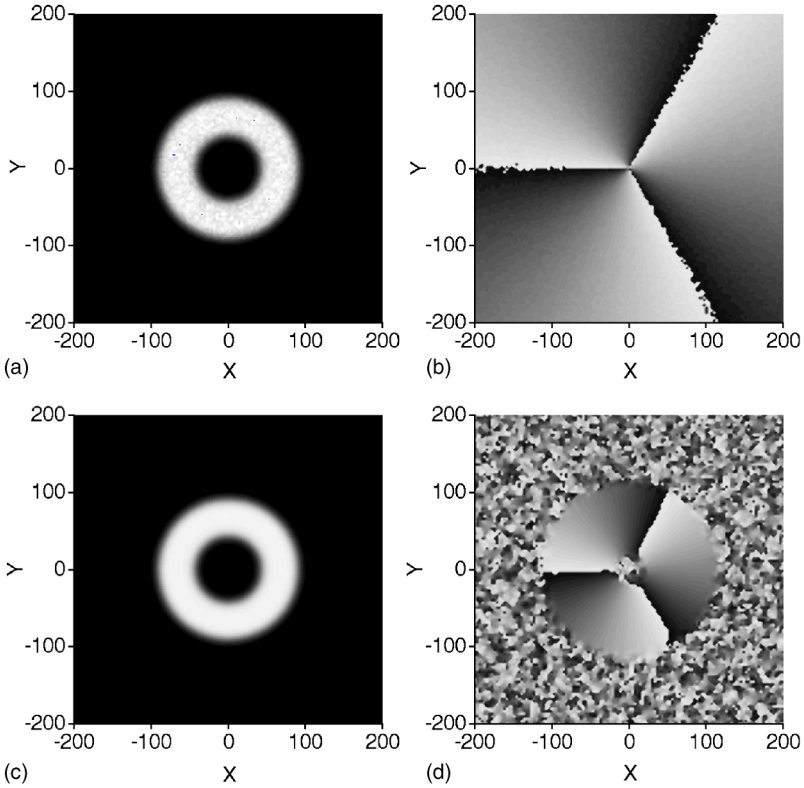

FIG. 11. Grey-scale plots illustrating the recovery of the perturbed stable $S=3$ soliton in the case of $\beta=0.2$ and $\kappa=0.0276$. (a) and (b) Intensity and phase distributions in the initial soliton with random noise added. (c) and (d) The same in the self-cleaned soliton at $Z=4500$.

shape is far from the soliton's exact form. Figure 12 demonstrates strong reshaping of the input pulse in the course of its self-trapping into the solitons, which leads to redistribution of the energy between the FF and SH components; some energy loss occurs, caused by emission of radiation in the course of the formation of the stable vortex soliton with $S=3$.

V. QUALITATIVE ANALYSIS OF STABILITY OF THE VORTEX SOLITONS

All the above results were obtained in a numerical form. While the predictions based on the stability eigenvalues match to direct simulations quite well, it is desirable to develop a qualitative understanding of the stability of the spinning solitons, based on sufficiently simple arguments. One approach to this problem was proposed in Ref. [8], where it was shown that the ring-shaped vortex may develop an instability against spontaneous shift of the inner hole from its central position, as the hole is attracted by the outer rim. However, this is only one of possible instability modes, and comparison with numerical simulations showed that it plays a dominant role rather seldom [8].

A simpler but more general analysis may be based on considering the vortex soliton as a two-dimensional "liquid drop" of the annular shape, with inner and outer borders. Then, an obvious stability criterion is minimization of the " surface tension," i.e., of the total length (perimeter) of the borders (the total area of the drop, or of a set of secondary drops into which the original unstable one may split, as shown above, is approximately conserved due to the power conservation). The outer and inner radii of the annulus being R [see Eq. (8)] and ρ, its area and perimeter are

$$S=\pi(R^2-\rho^2), \quad L=2\pi(R+\rho). \tag{13}$$

If the annular drop is unstable against splitting into n round-shaped ones with a radius $\tilde{R}$ (like, for instance, in the case shown in Fig. 9), the area conservation yields $\tilde{R}=\sqrt{S/(\pi n)}=\sqrt{(R^2-\rho^2)/n}$. Accordingly, the total perimeter of the set of the secondary drops is

$$l\equiv 2\pi\tilde{R}n=2\pi\sqrt{n(R^2-\rho^2)}. \tag{14}$$

As it follows from Eqs. (13) and (14), the ratio of the perimeters of the split and unsplit configurations is

$$\frac{l}{L}=\sqrt{n\frac{R-\rho}{R+\rho}}. \tag{15}$$

An obvious consequence of Eq. (15) is that the condition $l/L>1$, which implies absolute stability of the annulus against the splitting into n drops, is

$$R>\frac{n+1}{n-1}\rho. \tag{16}$$

The strongest condition following from Eq. (16) corresponds to $n=2$ (recall that the exact numerical results demonstrate that the instability mode with the azimuthal index $n=2$, which implies the beginning of the splitting into two fragments, is indeed the most persistent one),

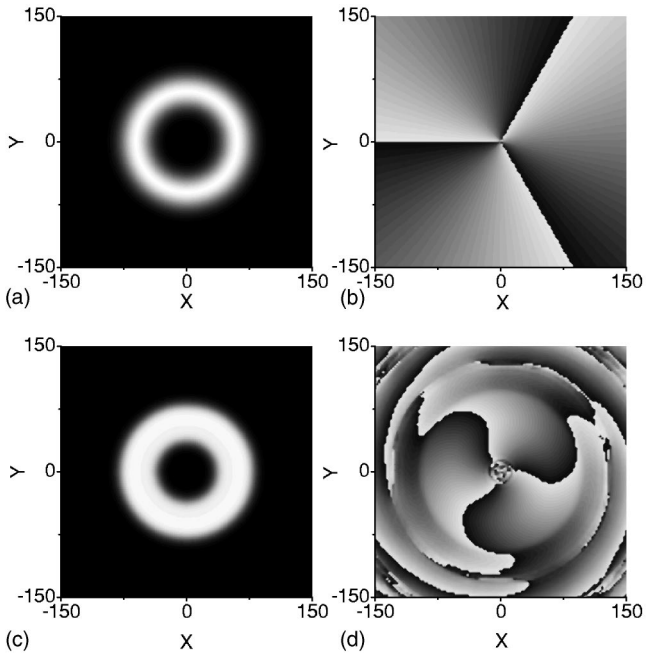

FIG. 12. Formation of the stable soliton with $S=3$ from a Gaussian input pulse with the trapped phase dislocation and initial power $E=885$. The mismatch is $\beta=0.2$. (a) and (b) The intensity and phase distributions in the initial Gaussian with a nested vortex. (c) and (d) The intensity and phase distributions in the spinning soliton at $Z=4000$.

$$R > 3\rho. \tag{17}$$

For κ sufficiently close to κ_{offset}, ρ depends only on the vorticity S of the annular soliton, while R may be indefinitely large, depending on the soliton's power. Thus, the condition (17) predicts that the vortex solitons of a sufficiently large size may indeed be stable against the splitting.

Further, to estimate the dependence of the stability region on S, we may use a crude estimate for ρ, following from the matching of the asymptotic form of the solution valid for $r \to 0$,

$$U(r) = ar^S, \quad V(r) = br^{2S}, \tag{18}$$

with some constants a and b [see Eqs. (2)], to the nearly "flat-top" solution in the inner region of the broad annular soliton. The latter solution may be approximated, for large r, by $U(r)=U_0+U_1S^2r^{-2}$, $V(r)=V_0+V_1S^2r^{-2}$, where U_0 and V_0 are the same as in Eqs. (6) and (7), while expressions for the constants U_1 and V_1 are available but cumbersome. For a crude estimate, we demand the continuity of the logarithmic derivatives, $U'(r)/U(r)$ and $V'(r)/V(r)$, at $r=\rho$, as following from the latter expressions, which are valid inside the flat-top region, and from the expressions (18), which describe the fields inside the hole. This procedure predicts the following dependence of the hole's radius on large values of S,

$$\rho = \rho_0\sqrt{S}, \tag{19}$$

with a constant ρ_0. The fact that the model must be based on competing self-focusing and self-defocusing nonlinearities implicitly comes into the play at this stage of the consideration, as otherwise the quasi-flat field in the inner region of the annulus would be subject to the modulational instability.

Finally, the relations (8), (17), and (19) that the relative size of the *stability region* for the vortex solitons shrinks, with the increase of S, as

$$\Delta\kappa/\kappa_{\text{offset}} \sim \exp(-C\sqrt{S}), \tag{20}$$

with a certain constant C. In fact, the prediction (20) is *universal* (model-independent), while C may depend on parameters of the particular model, such the mismatch constant β in the present $\chi^{(2)}:\chi^{(3)}_{-}$ system. The numerical results quoted above for $1 \leqslant S \leqslant 4$ are not quite sufficient to check Eq. (20), as these values of S may not be large enough. Nevertheless, even these data are not incompatible with the prediction: in the case of $\beta=+0.2$, the results for S ranging between 2 and 4 (obviously, the case of $S=1$ should be excluded) imply C taking values between 1.94 and 2.07, and similar results for $\beta=-0.05$ imply that C varies between 2.03 and 2.17.

VI. CONCLUSION

In this work, we have revisited the earlier considered problem of stability of vortex solitons in two-dimensional media combining the quadratic and self-defocusing cubic $[\chi^{(2)}:\chi^{(3)}_{-}]$ nonlinearities. The model describes propagation of localized beams with intrinsic vorticity S in the bulk optical medium. An earlier established result was that the vortex solitons with $S=1$ and $S=2$ could be stable, provided that their external size and power are large enough, but it was assumed that all the higher-order solitons with $S \geqslant 3$ would be unstable. In contrast with this, it has recently been found that in another model, with the cubic-quintic nonlinearity, solitons with $S>2$ had their (narrow) stability regions, too. In this work, we have demonstrated that the same is true in the $\chi^{(2)}:\chi^{(3)}_{-}$ model, too. In particular, the $S=3$ and $S=4$ solitons are stable in regions which occupy, respectively, $\simeq 3\%$ and 1.5% of their existence domain. Solitons with still larger S also have very narrow stability regions. These results were obtained by means of calculation of the stability eigenvalues, and checked in direct simulations. It has also been demonstrated that the stable solitons are truly robust, readily self-trapping from a rather arbitrary initial beam with the embedded vorticity, and easily cleaning themselves from large random perturbations. The dependence of the stability on the $\chi^{(2)}$ phase-mismatch coefficient, which is the most important control parameter of the model, was investigated.

Besides the numerical results, we have also proposed a simple qualitative explanation for the stability of the broad vortices against splitting into a set of zero-spin solitons. In particular, this analysis predicts that, for large S, the width of stability region shrinks according to Eq. (20).

Thus, we conclude that the stability of higher-order two-dimensional spinning solitons is a *generic feature* of media with competing self-focusing and self-defocusing nonlinearities, as it takes place in both the cubic-quintic and $\chi^{(2)}:\chi^{(3)}_{-}$

ones. A remaining challenge is possible stability of *three-dimensional* spinning solitons with $S>1$ in media with competing nonlinearities; recall that three-dimensional spinning solitons (vortex tori) with topological charge $S=1$ have their stability region in such models [21].

ACKNOWLEDGMENTS

We appreciate valuable discussions with R. L. Pego. D. Mihalache and D. Mazilu acknowledge support from Deutsche Forschungsgemeinschaft (DFG), Germany.

[1] A. G. Truscott, M. E.J. Friese, N. R. Heckenberg, and H. Rubinsztein-Dunlop, Phys. Rev. Lett. **82**, 1438 (1999).
[2] C. T. Law, X. Zhang, and G. A. Swartzlander, Opt. Lett. **25**, 55 (2000).
[3] G. A. Swartzlander and C. T. Law, Phys. Rev. Lett. **69**, 2503 (1992); A. W. Snyder, L. Poladian, and D. J. Mitchell, Opt. Lett. **17**, 789 (1992); D. Rozas, C. T. Law, and G. A. Swartzlander, J. Opt. Soc. Am. B **14**, 3504 (1997); B. Luther-Davies, J. Christou, V. Tikhonenko, and Yu. S. Kivshar, *ibid.* **14**, 3045 (1997); Yu. S. Kivshar, J. Christou, V. Tikhonenko, B. Luther-Davies, and L. Pismen, Opt. Commun. **152**, 198 (1998).
[4] V. Y. Bazhenov, M. S. Soskin, and M. V. Vasnetsov, J. Mod. Opt. **39**, 985 (1992); M. S. Soskin and M. V. Vasnetsov, Pure Appl. Opt. **7**, 301 (1998).
[5] V. I. Kruglov and R. A. Vlasov, Phys. Lett. **111A**, 401 (1985).
[6] M. Quiroga-Teixeiro and H. Michinel, J. Opt. Soc. Am. B **14**, 2004 (1997).
[7] I. Towers, A. V. Buryak, R. A. Sammut, B. A. Malomed, L.-C. Crasovan, and D. Mihalache, Phys. Lett. A **288**, 292 (2001); D. Mihalache, D. Mazilu, I. Towers, B. A. Malomed, and F. Lederer, J. Opt. A, Pure Appl. Opt. **4**, 615 (2002).
[8] B. A. Malomed, L.-C. Crasovan, and D. Mihalache, Physica D **161**, 187 (2002).
[9] H. Michinel, J. Campo-Táboas, M. L. Quiroga-Teixeiro, J. R. Salgueiro, and R. García-Fernández, J. Opt. B: Quantum Semiclassical Opt. **3**, 314 (2001).
[10] V. I. Berezhiani, V. Skarka, and N. B. Aleksic, Phys. Rev. E **64**, 057601 (2001).
[11] R. L. Pego and H. A. Warchall, J. Nonlinear Sci. **12**, 347 (2002).
[12] T. A. Davydova, A. I. Yakimenko, and Yu. A. Zaliznyak, Phys. Rev. E **67**, 026402 (2003).
[13] L.-C. Crasovan, B. A. Malomed, and D. Mihalache, Pramana, J. Phys. **57**, 1041 (2001); B. A. Malomed, G. D. Peng, P. L. Chu, I. Towers, A. V. Buryak, and R. A. Sammut, *ibid.* **57**, 1061 (2001).
[14] L.-C. Crasovan, B. A. Malomed, and D. Mihalache, Phys. Rev. E **63**, 016605 (2001); Phys. Lett. A **289**, 59 (2001).
[15] P. Di Trapani, W. Chinaglia, S. Minardi, A. Piskarskas, and G. Valiulis, Phys. Rev. Lett. **84**, 3843 (2000).
[16] I. Towers, A. V. Buryak, R. A. Sammut, and B. A. Malomed, Phys. Rev. E **63**, 055601(R) (2001).
[17] A. S. Desyatnikov and Yu. S. Kivshar, Phys. Rev. Lett. **87**, 033901 (2001).
[18] Z. H. Musslimani, M. Soljacic, M. Segev, and D. N. Christodoulides, Phys. Rev. E **63**, 066608 (2001).
[19] A. Desyatnikov, A. Maimistov, and B. Malomed, Phys. Rev. E **61**, 3107 (2000); D. Mihalache, D. Mazilu, L.-C. Crasovan, B. A. Malomed, and F. Lederer, *ibid.* **61**, 7142 (2000).
[20] D. Mihalache, D. Mazilu, L.-C. Crasovan, B. A. Malomed, and F. Lederer, Phys. Rev. E **62**, R1505 (2000).
[21] D. Mihalache, D. Mazilu, L.-C. Crasovan, I. Towers, A. V. Buryak, B. A. Malomed, L. Torner, J. P. Torres, and F. Lederer, Phys. Rev. Lett. **88**, 073902 (2002); D. Mihalache, D. Mazilu, L.-C. Crasovan, I. Towers, B. A. Malomed, A. V. Buryak, L. Torner, and F. Lederer, Phys. Rev. E **66**, 016613 (2002); D. Mihalache, D. Mazilu, I. Towers, B. A. Malomed, and F. Lederer, *ibid.* **67**, 056608 (2003).
[22] Yu. S. Kivshar and G. P. Agrawal, *Optical Solitons: From Fibers to Photonics Crystals* (Academic, Amsterdam, 2003).
[23] K. T. Gahagan and G. A. Swartzlander, J. Opt. Soc. Am. B **16**, 533 (1999).
[24] H. He, M. E.J. Friese, N. R. Heckenberg, and H. Rubinsztein-Dunlop, Phys. Rev. Lett. **75**, 826 (1995).
[25] C.-C. Jeng, M.-F. Shih, K. Motzek, and Y. Kivshar, Phys. Rev. Lett. **92**, 043904 (2004).
[26] D. V. Petrov, L. Torner, J. Martorell, R. Vilaseca, J. P. Torres, and C. Cojocaru, Opt. Lett. **23**, 1444 (1998).
[27] M. S. Bigelow, P. Zerom, and R. W. Boyd, Phys. Rev. Lett. **92**, 083902 (2004).
[28] N. G. Vakhitov and A. A. Kolokolov, Radiophys. Quantum Electron. **16**, 783 (1975); A. A. Kolokolov, Lett. Nuovo Cimento Soc. Ital. Fis. **8**, 197 (1973).
[29] L. Torner and D. V. Petrov, Electron. Lett. **33**, 608 (1997); W. J. Firth and D. V. Skryabin, Phys. Rev. Lett. **79**, 2450 (1997); D. V. Skryabin and W. J. Firth, Phys. Rev. E **58**, 3916 (1998); L. Torner, J. P. Torres, D. V. Petrov, and J. M. Soto-Crespo, Opt. Quantum Electron. **30**, 809 (1998).
[30] A. V. Buryak, Yu. S. Kivshar, and S. Trillo, Opt. Lett. **20**, 1961 (1995); M. A. Karpierz, *ibid.* **20**, 1677 (1995).
[31] O. Bang, Yu. S. Kivshar, and A. V. Buryak, Opt. Lett. **22**, 1680 (1997); O. Bang, J. Opt. Soc. Am. B **14**, 51 (1997); L. Bergé, O. Bang, J. J. Rasmussen, and V. K. Mezentsev, Phys. Rev. E **55**, 3555 (1997); O. Bang, Yu. S. Kivshar, A. V. Buryak, A. De Rossi, and S. Trillo, *ibid.* **58**, 5057 (1998).
[32] L. Torner, IEEE Photonics Technol. Lett. **11**, 1268 (1999); O. Bang, C. Clausen, P. Christiansen, and L. Torner, Opt. Lett. **24**, 1413 (1999); J. F. Corney and O. Bang, Phys. Rev. E **64**, 047601 (2001); N.-C. Panoiu, D. Mihalache, D. Mazilu, F. Lederer, and R. M. Osgood, *ibid.* **68**, 016608 (2003); N.-C. Panoiu, D. Mihalache, H. Rao, and R. M. Osgood, *ibid.* **68**, 065603(R) (2003); S. K. Johansen, S. Carrasco, L. Torner, and O. Bang, Opt. Commun. **203**, 393 (2002).
[33] D. Rozas, C. T. Law, and G. A. Swartzlander, J. Opt. Soc. Am. B **14**, 3054 (1997).
[34] B. A. Malomed, P. Drummond, H. He, A. Berntson, D. Anderson, and M. Lisak, Phys. Rev. E **56**, 4725 (1997); D. V. Skryabin and W. J. Firth, Opt. Commun. **148**, 79 (1998); D. Mihalache, D. Mazilu, B. A. Malomed, and L. Torner, *ibid.* **152**,

365 (1998); D. Mihalache, D. Mazilu, J. Dörring, and L. Torner, *ibid.* **159**, 129 (1999); L. Torner, S. Carrasco, J. P. Torres, L.-C. Crasovan, and D. Mihalache, *ibid.* **199**, 277 (2001).

[35] D. Mihalache, D. Mazilu, B. A. Malomed, and L. Torner, Opt. Commun. **169**, 341 (1999); D. Mihalache, D. Mazilu, L.-C. Crasovan, L. Torner, B. A. Malomed, and F. Lederer, Phys. Rev. E **62**, 7340 (2000).

[36] A. V. Buryak, P. Di Trapani, D. V. Skryabin, and S. Trillo, Phys. Rep. **370**, 63 (2002); C. Etrich, F. Lederer, B. A. Malomed, T. Peschel, and U. Peschel, Prog. Opt. **41**, 483 (2000).

[37] L. Torner, D. Mazilu, and D. Mihalache, Phys. Rev. Lett. **77**, 2455 (1996); C. Etrich, U. Peschel, F. Lederer, and B. A. Malomed, Phys. Rev. E **55**, 6155 (1997).

[38] N. N. Akhmediev and A. Ankiewicz, *Solitons, Nonlinear Pulses and Beams* (Chapman and Hall, London, 1997).

[39] L. Allen, M. J. Padgett, and M. Babiker, Prog. Opt. **39**, 291 (1999).

[40] G. Dahlquist and Å. Björk, *Numerical Methods* (Prentice Hall, Englewood Cliffs, NJ, 1974).

[41] J. M. Soto-Crespo, D. R. Heatley, E. M. Wright, and N. N. Akhmediev, Phys. Rev. A **44**, 636 (1991); J. Atai, Y. Chen, and J. M. Soto-Crespo, *ibid.* **49**, R3170 (1994).

[42] N. N. Akhmediev, A. Ankiewicz, and H. T. Tran, J. Opt. Soc. Am. B **10**, 230 (1993).

[43] I. V. Barashenkov, D. E. Pelinovsky, and E. V. Zemlyanaya, Phys. Rev. Lett. **80**, 5117 (1998); A. De Rossi, C. Conti, and S. Trillo, *ibid.* **81**, 85 (1998); J. Schöllmann, R. Scheibenzuber, A. S. Kovalev, A. P. Mayer, and A. A. Maradudin, Phys. Rev. E **59**, 4618 (1999).

[44] D. Mihalache, D. Mazilu, and L. Torner, Phys. Rev. Lett. **81**, 4353 (1998); D. Mihalache, D. Mazilu, and L.-C. Crasovan, Phys. Rev. E **60**, 7504 (1999).

[45] J. M. Ortega and W. C. Rheinboldt, *Iterative Solution of Nonlinear Equations in Several Variables* (Academic, New York, 1970), p. 182.

[46] D. E. Edmundson, Phys. Rev. E **55**, 7636 (1997).